THE JOURNAL OF BIOLOGICAL CHEMISTRY VOL. 281, NO. 18, pp. 12751–12759, May 5, 2006

Posttranslational Cleavage and Adaptor Protein Complex-dependent Trafficking of Mucolipin-1*

Received for publication, October 12, 2005, and in revised form, February 28, 2006 Published, JBC Papers in Press, March 3, 2006, DOI 10.1074/jbc.M511104200

Mark T. Miedel[‡], Kelly M. Weixel[‡1], Jennifer R. Bruns[‡], Linton M. Traub[§], and Ora A. Weisz[‡§2]

From the [‡]Renal-Electrolyte Division, Department of Medicine, and [§]Department of Cell Biology and Physiology, University of Pittsburgh, Pittsburgh, Pennsylvania 15261

Mucolipin-1 (ML1) is a member of the transient receptor potential ion channel superfamily that is thought to function in the biogenesis of lysosomes. Mutations in ML1 result in mucolipidosis type IV, a lysosomal storage disease characterized by the intracellular accumulation of enlarged vacuolar structures containing phospholipids, sphingolipids, and mucopolysaccharides. Little is known about how ML1 trafficking or activity is regulated. Here we have examined the processing and trafficking of ML1 in a variety of cell types. We find that a significant fraction of ML1 undergoes cell type-independent cleavage within the first extracellular loop of the protein during a late step in its biosynthetic delivery. To determine the trafficking route of ML1, we systematically examined the effect of ablating adaptor protein complexes on the localization of this protein. Whereas ML1 trafficking was not apparently affected in fibroblasts from *mocha* mice that lack functional adaptor protein complex (AP)-3, small interfering RNA-mediated knockdown revealed a requirement for AP-1 in Golgi export of ML1. Knockdown of functional AP-2 had no effect on ML1 localization. Interestingly, cleavage of ML1 was not compromised in AP-1-deficient cells, suggesting that proteolysis occurs in a prelysosomal compartment, possibly the *trans*-Golgi network. Our results suggest that posttranslational processing of ML1 is more complex than previously described and that this protein is delivered to lysosomes primarily via an AP-1-dependent route that does not involve passage via the cell surface.

Mucolipidosis type IV (MLIV)[3] is an autosomal recessive lysosomal storage disorder characterized clinically by developmental abnormalities of the brain, impaired neurological and gastric functions, and ophthalmologic defects that include corneal opacity and retinal degeneration (1). At the cellular level, lysosomal storage bodies appearing as enlarged vacuolar structures are found in every cell type of affected individuals, with the accumulated products including a broad range of phospholipids, sphingolipids, and mucopolysaccharides (1, 2). Other classes of mucolipidoses include sialidosis (type I), I-cell disease (type II), and pseudo-Hurler polydystrophy (type III), where accumulation is a result of impaired targeting of the lysosomal hydrolases involved in the catabolism of the stored lipids. However, lysosomal hydrolase activity is not impaired in MLIV, since the accumulated lipid products have been previously shown to be catabolized normally (3). Rather, MLIV pathophysiology has been linked to mutations in the transient receptor potential (TRP) channel family member mucolipin-1 (TRPML subfamily; herein referred to as ML1), where mutations result in a defect in membrane sorting along the late endocytic pathway (4–6).

Mammalian TRP channels are a large class of proteins that are characterized by a common structure and permeability to both monovalent cations and Ca^{2+} ions (7–9). At least 20 mammalian TRP channels have been identified that comprise six TRP subfamilies. TRPs have widespread tissue distributions and have been implicated in diverse cellular functions, including roles in mechanosensation, osmosensation, sensation of fluid flow in vascular endothelia, sensation of temperature, pain, and touch, and transepithelial transport of Ca^{2+} and Mg^{2+} (7–9). Specifically, mucolipin-1 (ML1) is a 580-amino acid protein that has a molecular mass of 65 kDa and has been localized to late endosomes/lysosomes in several cell types (10). Two other mammalian mucolipin family members have also been identified, ML2 and ML3. Whereas little is known regarding ML2 function, mutations in the mouse *Mcoln3* gene are associated with deafness and pigmentation defects in varitint-waddler (Va) mice (11). ML1 is suggested to be a multiple subconductance and nonspecific cation channel, where activity is modulated by both Ca^{2+} and pH (12, 13), indicating that this protein may be involved in trafficking or fusion events between late endosomes and lysosomes in the late endocytic pathway (14, 15). ML1 has six predicted transmembrane-spanning segments and is oriented with both the amino and carboxyl termini in the cytoplasm (Fig. 4*A*), a characteristic trait of all TRP channel family members. The TRP domain of ML1 spans transmembrane segments 3–6 with the pore region occurring between the fifth and sixth segments. Additionally, ML1 has a large extracellular loop, located between the first and second transmembrane segments that has four consensus *N*-linked glycosylation sites. Among other TRP family members, only polycystin-2 (TRPP subfamily) shares this feature of having a large extracellular loop. It is thought that this large extracellular loop may be involved in channel activation, since both ML1 and polycystin-2 have relatively short amino- and carboxyl-terminal cytoplasmic tails that often serve as activation regions for other cation channels. ML1 also has a carboxyl-terminal dileucine targeting motif that has been postulated to serve as the lysosomal targeting signal for ML1 (4, 5).

Much of what is presently known regarding ML1 has come from studies in *Caenorhabditis elegans* where the ML1 functional orthologue, CUP-5, has been identified. Mutations in the *cup-5* gene have been described to cause a defect in lysosome biogenesis, since CUP-5 is localized to both late endosome-lysosome fusion sites as well as to mature lysosomes. The observed endocytic abnormalities observed in *cup-5* mutants were rescued upon the addition of either human ML1 or ML3 (16). Therefore, it is hypothesized that ML1 may be responsible for regulating fusion events during the biogenesis of lysosomes (16–18).

* This work was supported by National Institutes of Health Grant R01-DK54407 (to O. A. W.). The costs of publication of this article were defrayed in part by the payment of page charges. This article must therefore be hereby marked "*advertisement*" in accordance with 18 U.S.C. Section 1734 solely to indicate this fact.
[1] Supported by National Institutes of Health T32-DK61296.
[2] To whom correspondence should be addressed: Renal-Electrolyte Division University of Pittsburgh, 3550 Terrace St., Pittsburgh, PA 15261. Tel.: 412-383-8891; Fax: 412-383-8956; E-mail: weisz@pitt.edu.
[3] The abbreviations used are: MLIV, mucolipidosis type IV; TRP, transient receptor potential; AP, adaptor protein; DMEM, Dulbecco's modified Eagle's medium; FBS, fetal bovine serum; GGA, Golgi-localized, γ-ear-containing, ARF-binding; HRP, horseradish peroxidase; ML1 mucolipin-1; HA, hemagglutinin; PBS, phosphate-buffered saline; siRNA, small interfering RNA.

However, little is known about how ML1 is targeted to late endosomes/lysosomes or how this ion channel may function to regulate membrane trafficking events along this pathway.

Here, we have investigated the posttranslational processing and trafficking of ML1. We find that ML1 is cleaved at a site between the second and third *N*-glycans of the first extracellular loop. Delivery of ML1 to lysosomes occurs via a direct pathway dependent on adaptor protein complex-1 (AP-1) and does not involve passage via the cell surface. ML1 cleavage occurs late in the biosynthetic pathway, after the glycans have been sialylated, but prior to lysosomal delivery, since inhibition of lysosomal delivery does not prevent cleavage. The apparently exclusive requirement for AP-1 in ML1 delivery suggests that surface delivery of this channel may have physiologically detrimental effects on cells.

MATERIALS AND METHODS

DNA Constructs—Constructs encoding human ML1 (corresponding to accession number BC005149) double-tagged with HA at the amino terminus and with Myc upstream of the carboxyl-terminal dileucine motif, or tagged individually with HA or Myc epitopes were provided by Kirill Kiselyov (28). A double-tagged ML1 construct in which a premature stop codon was inserted into the ML1 open reading frame prior to the lysine residue at amino acid position 577 (ML1 ΔLLVN) was also a gift of Dr. Kiselyov.

Site-directed Mutagenesis—The mutations N179A, N220A, N230A, R200A, and K219A were generated using the QuikChange site-directed mutagenesis kit (Stratagene) according to the manufacturer's protocol. Mutations and overall plasmid integrity were confirmed by direct DNA sequencing. The following forward (F) and reverse (R) primer pairs were used to introduce the desired mutations: N179A (F), 5′-CGTGGACCCGGCCGCCGACACATTTGAC-3′; N179A (R), 5′-GTCAAATGTGTCGCGGGCCGGGTCCACG-3′; N220A (F), 5′-GGAAAGCAGCTCCAGTTACAAGGCCCTCACGCTC-3′; N220A (R), 5′-GAGCGTGAGGGCCTTGTAACTGGAGCTGCTTTCC-3′; N230A (F), 5′-CCACAAGCTGGTCGCTGTCACCATCCACTTCC-3′; N230A (R), 5′-GGAAGTGGATGGTGACAGCGACCAGCTTGTGG-3′; R200A (F), 5′-GATCCCCCCGAGGCGCCCCCTCCGCC-3′; R200A (R), 5′-GGCGGAGGGGGCGCCTCGGGGGGATC-3′; K219A (F), 5′-GGAAAGCAGCTCCAGTTACGCGAACCTCACGCTCAAATT-3′; K219A (R), 5′-GAATTTGAGCGTGAGGTTCGCGTAACTGGAGCTGCTTTCC-3′.

Insertion of an External HA Epitope Tag—We used a modified version of the QuikChange (Stratagene) site-directed mutagenesis protocol (19) to incorporate an HA epitope tag into the first extracellular loop between amino acids 249 (Glu) and 250 (Ile) of Myc-tagged ML1 (referred to as ML1-HA(ext)). The following primers were used (underlined and boldface text indicate nucleotides corresponding to the HA epitope sequence): forward, 5′-CAGAGCCTCATCAATAATGAG**ATGTACCCATACGATGTTCCAGATTACGCT**ATCCCGGACTGCTATACCTTC-3′; reverse, 5′-GAAGGTATAGCAGTCCGGGAT**AGCGTAATCTGGAACATCGTATGGGTACAT**CTCATTATTGATGAGGCTCTG-3′.

Cell Culture and Transient Transfection—HEK293 and HeLa SS6 cells were maintained in Dulbecco's modified Eagle's medium (DMEM) supplemented with 10% fetal bovine serum (FBS) and 100 μg/ml penicillin/streptomycin. Primary cultures of rabbit cornea epithelial cells were provided by Emily Guerriero and Nirmala SundarRaj and were maintained in DMEM-F-12 supplemented with 40 μg/ml gentamicin, 0.5% Me_2SO, 5 μg/ml bovine insulin, 10 ng/ml human epidermal growth factor, 0.1 μg/ml cholera toxin, 50 units/ml penicillin, 50 μg/ml streptomycin, and 8% FBS. NIH 3T3 and *mocha* fibroblasts were provided by Gudrun Ihrke and were maintained in DMEM supplemented with 10% FBS and 100 μg/ml penicillin and streptomycin. For transient transfections, cells were plated in either 6- or 24-well plates at 30% confluence and incubated until cells reached ~75–80% confluence. Transient transfections using Lipofectamine 2000 (Invitrogen) were performed according to the manufacturer's protocol. For HEK293 cells or fibroblasts cultured in 6-well plates, the DNA/Lipofectamine 2000 ratio used was 2 μg of DNA to 5 μl of Lipofectamine. For HeLa SS6 cells or fibroblasts grown in 24-well plates, the ratio used was 0.8 μg of DNA to 2 μl of Lipofectamine 2000.

Immunoblotting of ML1—Transiently transfected cells were solubilized in 1.5% (v/v) C12E9 (Calbiochem) in buffer containing 150 mM NaCl, 1 mM EDTA, and 40 mM HEPES, pH 7.4. This detergent solution was additionally supplemented with 1 μg/ml aprotinin and complete mini-EDTA-free protease inhibitor mixture tablets (Roche Applied Science). Samples were immunoprecipitated using monoclonal anti-HA (HA.11; Covance) or monoclonal anti-c-Myc (Upstate Biotechnology, Inc., Lake Placid, NY) antibodies. Antibody-antigen complexes were recovered using Pansorbin cells (Calbiochem). Samples were then washed one time each in HBS (10 mM HEPES, 150 mM NaCl, pH 7.4) containing either 1% Triton X-100 or 0.01% SDS and then washed one final time in HBS alone. Samples were solubilized in Laemmli sample buffer and heated to 60 °C for 30 min and loaded onto 4–15% Tris-HCl precast gels (Bio-Rad). Electrophoresis and transfer to Highbond-ECL nitrocellulose membrane (Amersham Biosciences) was performed using the Criterion Western blotting system (Bio-Rad). Membranes were then incubated for 2 h with anti-HA-HRP or anti-c-Myc-HRP (Roche Applied Science). HRP-reactive bands were detected using Super Signal West Pico chemiluminescent substrate (Pierce), and membranes were exposed to Eastman Kodak Co. X-Omat Blue film. The relative molecular mass of immunoreactive bands was assessed using Precision Plus Protein Standards (Bio-Rad). Samples treated with *N*-glycanase (New England Biolabs) were immunoprecipitated with monoclonal anti-HA antibody, and immunocomplexes were recovered as described above. Samples were washed and eluted for 30 min at 60 °C with 10 mM Tris-HCl, pH 8.6, 0.2% SDS, and 7.5% glycerol. Following elution, samples were subjected to brief centrifugation, the supernatants were recovered, and 0.5 μl of *N*-glycanase (New England Biolabs; 1.5 units of active enzyme) was added to each sample. Control samples were treated identically except that *N*-glycanase was omitted from the incubation. Samples were incubated overnight at 37 °C unless otherwise indicated. The following day, 2-fold concentrated Laemmli sample buffer was added to each sample (to a final volume of 30 μl) and incubated at 60 °C for 30 min. Samples were electrophoresed on 4–15% Tris-HCl gels and immunoblotted as described above.

Metabolic Labeling of ML1—Transiently transfected HEK293 cells on 6-well plates were starved in cysteine- and methionine-free medium for 30 min and then radiolabeled with 1 mCi/ml Tran^{35}S-label (MP Biomedicals) for 2 h. Cells were chased in serum-free DMEM for 0 or 2 h and then solubilized, and ML1 was immunoprecipitated as described above. Samples were then either treated with *N*-glycanase as described above or directly solubilized in Laemmli sample buffer and incubated for 30 min at 60 °C prior to electrophoresis on 4–15% Tris-HCl gels. Dried gels were analyzed using a phosphor imager (Bio-Rad), and the relative molecular mass of visualized bands was compared with Rainbow [^{14}C]methylated protein molecular weight markers (Amersham Biosciences). Where indicated, the following drugs were added during both the radiolabeling and chase periods: leupeptin (Sigma; 20 μM), CA-074-Me (Calbiochem; 2 μM), and brefeldin A (Calbiochem; 10 μg/ml).

Indirect Immunofluorescence—Transiently transfected cells grown on coverslips were fixed with 4% paraformaldehyde, permeabilized with 0.1% Triton X-100 in PBS containing 1% bovine serum albumin, and incubated in blocking solution (PBS containing 1% bovine serum albumin) for 30 min. Samples were incubated for 60 min in primary antibody at the following dilutions: mouse monoclonal anti-HA (1:500); rat monoclonal anti-HA (clone 3F10; Roche Applied Science) (1:250); polyclonal anti-cathepsin D generated against the human peptide (20) (1:250); monoclonal AP.6 directed against AP-2 α subunit (American Type Culture Collection) (1:10); monoclonal anti-γ-adaptin (BD Biosciences) (1:250); monoclonal anti-giantin (1:400) (gift from Dr. Adam Linstedt, Carnegie Mellon University, Pittsburgh, PA), and monoclonal anti-lamp-2 directed against either the human epitope (H4B4) or mouse epitope (ABL-93) (Developmental Studies Hybridoma Bank, Iowa City, IA) (developed by J. Thomas August) (1:10). After washing, samples were incubated for 60 min with species-appropriate secondary antibodies conjugated to either AlexaFluor-488 or AlexaFluor-647 (Invitrogen or Molecular Probes) diluted in blocking buffer (1:500). Confocal imaging was performed on an Olympus IX-81 (Melville, NY) equipped with an UltraView spinning disc confocal head (PerkinElmer Life Sciences) and an argon-ion, argon-krypton, and helium-cadmium laser combiner. Images were acquired with a ×60 or ×100 plan-apochromat objective (numerical aperture 1.4) and the appropriate filter combination. The TIFF images were imported into Adobe Photoshop (Adobe, Mountain View, CA) to adjust contrast and image size.

Antibody Uptake Assay—NIH 3T3 or *mocha* fibroblasts grown on coverslips were transfected where indicated to express ML1-HA(ext). Cells were incubated for 1 h at 37 °C in the presence of appropriate antibodies (monoclonal HA for ML1-HA(ext)-transfected cells or anti-murine lamp-2 (ABL-93; Developmental Studies Hybridoma Bank) for untransfected cells) diluted to 50 μg/ml in DMEM containing 1% bovine serum albumin and 25 mM HEPES, pH 7.4. Leupeptin (20 μM) was included during the incubation to minimize degradation of any lysosomally delivered antibody. Cells were then washed three times with ice-cold PBS, fixed with 4% paraformaldehyde for 10 min, quenched with PBS-glycine, permeabilized for 3 min with 0.5% Triton X-100, and blocked for 15 min in blocking solution. Following block, cells were incubated with fluorophore-conjugated secondary antibody and processed for immunofluorescence as described above.

siRNA-mediated Knockdown of AP-1 γ and AP-2 α Subunits—Double-stranded siRNAs targeting human forms of either the AP-1 γ or AP-2 α subunit were purchased from Dharmacon (Lafayette, CO). For the AP-1 γ subunit, the target sequence used was 5′-AAGTTCCTGAACTTATGGAGA-3′, corresponding to nucleotides 528–548 of the human AP-1 complex γ1 subunit mRNA (accession number Y12226). For the AP-2 α subunit, the target sequence used was 5′-GCATGTGCACGCTGGCCA-3′, corresponding to nucleotides 1233–1250 of the human AP-2 α2 subunit mRNA (accession number NM_012305) Three potential target sequences were tested in each case. HeLa SS6 cells were plated in 24-well dishes and allowed to grow to ~50% confluence. Cells were transfected with a nonsilencing negative control siRNA duplex (Qiagen) or siRNA oligonucleotides targeted against the γ-subunit of AP-1 and/or the α-subunit of AP-2 using the *Trans*IT-TKO oligonucleotide transfection reagent (Mirus). For single knockdowns, 3 μl of siRNA oligonucleotide (20 μM) and 4.5 μl of transfection reagent were added per well; for samples transfected with both α- and γ-siRNAs, 3 μl of each oligonucleotide and 4.5 μl of transfection reagent were added. After 24 h, cells were transfected with cDNA encoding double-tagged ML1 (0.8 μg) and Lipofectamine 2000 (2 μl) and allowed to grow for an additional 18–24 h. Cells were either processed for immunofluorescence as described above or for immunoblotting. For Western blotting, cells were trypsinized and quenched with an equal volume of DMEM, 10% FBS. After centrifugation, cell pellets were washed once with PBS and then solubilized in 95 °C 2-fold concentrated Laemmli sample buffer. After determination of relative protein concentrations by Coomassie stain, equal amounts of protein were loaded on a second 4–15% Tris-HCl gel and processed for Western blot using monoclonal anti-AP-2 α (Santa Cruz Biotechnology; 1:5000), polyclonal anti-AP-1 γ (AE/1; 1:2000) (21), and E7 anti-β-tubulin monoclonal antibody (1:5000; Developmental Studies Hybridoma Bank, Iowa City, IA; developed by M. Klymkosky). ML1 was detected in siRNA-treated samples after solubilization, immunoprecipitation, and immunoblotting as described above.

RESULTS AND DISCUSSION

ML1 Is Cleaved Late in the Biosynthetic Pathway—Western blot analysis of transiently expressed ML1 demonstrated multiple immunoreactive species that could represent proteolytic processing. To examine this further, we expressed a construct encoding ML1 containing an amino-terminal HA and an internal carboxyl-terminal Myc epitope tag in HEK293 cells. Cell lysates were immunoprecipitated with anti-HA antibody, immunoblotted using HRP-conjugated anti-HA, and then stripped and reprobed using HRP-conjugated anti-Myc antibody. As shown in Fig. 1*A*, full-length ML1 was detected using either antibody as a doublet at ~60–70 kDa that probably represents the immature and mature glycosylated forms of the protein. In addition, a ladder of more slowly migrating bands was also observed (see also Fig. 1*C*), consistent with multimerization of this highly hydrophobic protein. Numerous approaches to dissociate these multimers were unsuccessful. In the anti-HA blot, an additional band at ~37 kDa was detected, whereas when the same blot was reprobed with anti-Myc, a distinct band at ~40 kDa was seen. These data suggest that ML1 is cleaved into two roughly equally sized fragments that can be co-isolated upon immunoprecipitation with an antibody against the N-terminal tag. The same results were obtained when ML1 was immunoprecipitated using anti-Myc antibody (Fig. 1*C*). Consistent with its hydrophobic character, the carboxyl-terminal Myc-reactive product also appeared to be sensitive to aggregation, since bands corresponding to dimers and higher order multimers of this cleavage product were routinely visualized by antibodies against the Myc epitope.

To determine whether the proteolytic cleavage event occurs early or late in the biosynthetic processing of ML1, we radiolabeled HEK293 cells transiently expressing ML1 for 2 h and solubilized the cells after a 0- or 2-h chase period. Lysates were immunoprecipitated using either anti-HA or anti-Myc antibody and examined by SDS-PAGE. As shown in Fig. 1*B* (*top*), ML1 was initially precipitated as a ~65–75-kDa doublet representing immature and fully glycosylated (sialylated) full-length protein. After the 2-h chase period, the immature glycosylated form of ML1 was no longer detected, consistent with *N*-glycan processing. At this time point, a broad band migrating at ~40 kDa was also detected, presumably representing the amino- and carboxyl-terminal ML1 cleavage fragments, which migrate with similar mobility on SDS-PAGE. The appearance of these cleavage products concomitant with maturation of the glycans on ML1 strongly suggests that proteolysis occurs after sialylation rather than early in the biosynthetic pathway. To further examine ML1 processing, HEK293 cells were treated with brefeldin A to prevent transit of newly synthesized ML1 along the biosynthetic pathway. In cells treated with brefeldin A, both cleavage and *N*-glycan processing are abolished, as is indicated by the absence of the ~40-kDa cleavage product and the loss of the ~65–75-kDa doublet after the 2-h

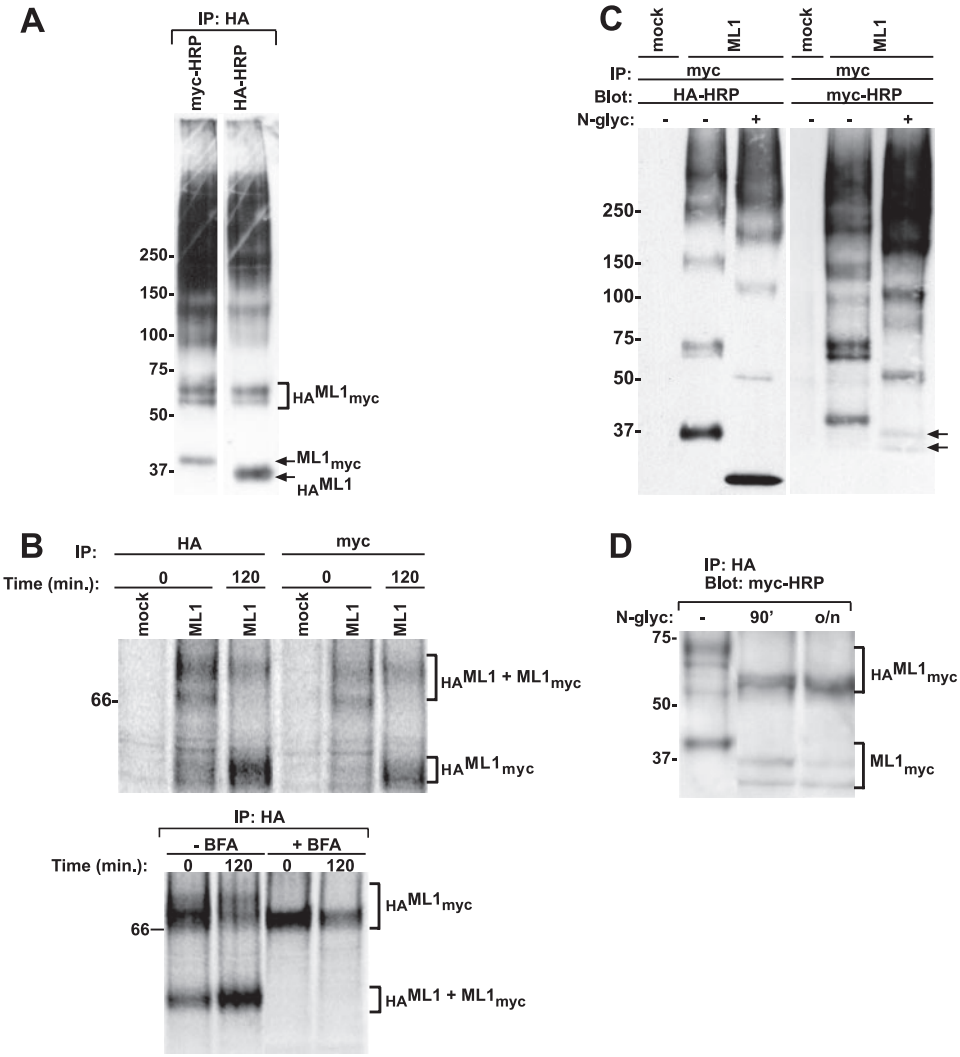

FIGURE 1. **ML1 is cleaved late in the biosynthetic pathway.** *A*, ML1 cleavage products co-precipitate. HEK293 cells transiently expressing double-epitope-tagged ML1 were solubilized and immunoprecipitated (*IP*) using anti-HA antibody. After SDS-PAGE on a 4–15% gradient gel, proteins were transferred to nitrocellulose and probed using HRP-conjugated anti-Myc (*left lane*). The same blot was then stripped and reprobed with HRP-conjugated anti-HA antibody (*right lane*). The migration of molecular weight standards is shown on the *left*. In this and subsequent figures, the band(s) corresponding to full-length double-tagged ML1 is labeled $_{HA}ML1_{myc}$, and those of the N- and C-terminal cleavage products are labeled $_{HA}ML1$ and $ML1_{myc}$, respectively. *B*, ML1 cleavage occurs late in the biosynthetic pathway. Mock-transfected or ML1-expressing cells were starved, radiolabeled for 2 h, and then chased for 0 or 2 h either in the absence or presence of brefeldin A (10 μg/ml; *lower panel*). Cells were solubilized, the lysates were immunoprecipitated using either anti-HA or anti-Myc antibody, and the samples were analyzed on 4–15% SDS-polyacrylamide gels. Note that $_{HA}$ML1 and $ML1_{Myc}$ cannot be individually resolved under these conditions. *C*, both N- and C-terminal ML1 cleavage products are glycosylated. Mock-transfected or ML1-expressing cells were solubilized, immunoprecipitated with anti-Myc antibody, and then either mock-treated or treated with *N*-glycanase prior to gel electrophoresis and blotting with either anti-HA or anti-Myc antibodies. The *arrows* indicate the $ML1_{Myc}$ doublet observed upon treatment with *N*-glycanase. *D*, lysates from ML1-expressing cells were immunoprecipitated with anti-Myc antibody and mock-treated (−) or treated with *N*-glycanase for 90 min or overnight prior to electrophoresis and immunoblotting using HRP-conjugated anti-Myc antibody. The $ML1_{Myc}$ doublet observed upon *N*-glycanase treatment appears to be due to incomplete cleavage of the *N*-glycans on this fragment, since longer incubation results in conversion of the more slowly migrating form to the more rapidly migrating form of the protein.

chase period (Fig. 1*B*, *bottom panel*). These results strongly suggest that cleavage of ML1 occurs at a post-ER site. Importantly, the cleavage site within ML1 appears to be cell type-independent, since similar products were observed when ML1 was expressed in several other cell types, including HeLa, Madin-Darby canine kidney, and rabbit cornea epithelial cells (Fig. 2).

Based on the sizes of the cleavage product, we hypothesized that cleavage occurs within the first, relatively large extracellular loop of ML1. This loop contains the only four potential *N*-glycosylation sites on ML1. Both cleavage products ($_{HA}$ML1 and $ML1_{Myc}$) were sensitive to *N*-glycanase treatment, confirming that cleavage occurs within this loop (Fig. 1*C*). Interestingly, we reproducibly found that *N*-glycanase treatment of the carboxyl-terminal half of the protein produced two distinct bands roughly 3 and 6 kDa smaller than the original fragment (indicated by *arrows*). These bands probably represent cleavage of either one or two *N*-glycans from this fragment, respectively. Longer treatments with *N*-glycanase demonstrated a precursor product relationship between the two, suggesting that cleavage of one of the *N*-glycans in this fragment is considerably more efficient than the other (Fig. 1*D*). We never observed complete conversion to the more rapidly migrating form, even when the *N*-glycanase treatment was carried out overnight and spiked with fresh enzyme.

Cleavage of ML1 Occurs between the Second and Third N-Glycans of the First Extracellular Loop—Our initial *N*-glycanase experiments suggest that the carboxyl-terminal fragment of ML1 contains at least two *N*-glycans. To test this more directly, we used site-directed mutagenesis to disrupt the *N*-glycosylation consensus sequences of the second, third, or fourth *N*-glycan and examined the effect of these mutations on the electrophoretic mobility of the HA- and Myc-tagged fragments immunoprecipitated from transiently transfected cells. As shown in Fig. 3,

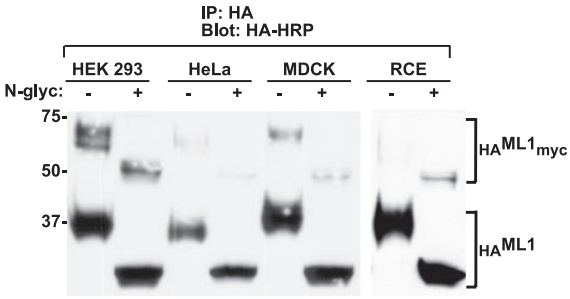

FIGURE 2. **Cleavage of ML1 is not cell type-specific.** The indicated immortalized cell lines or primary cultures of rabbit cornea epithelial cells (*RCE*) were transiently transfected to express $_{HA}ML1_{Myc}$. After solubilization, samples were immunoprecipitated (*IP*) using anti-HA antibody, mock-treated or treated with *N*-glycanase, and detected by immunoblotting using HRP-conjugated anti-HA antibody. *MDCK*, Madin-Darby canine kidney.

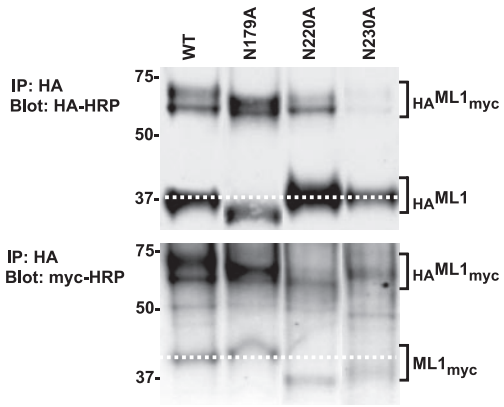

FIGURE 3. **Cleavage of ML1 occurs between the second and third *N*-glycans of the first extracellular loop.** Double-tagged wild-type ML1 or ML1 glycosylation mutants (N179A, N220A, and N230A) were transiently expressed in HEK293 cells. After solubilization, cell lysates were immunoprecipitated (*IP*) with anti-HA antibody, and samples were immunoblotted using HRP-conjugated anti-HA (*top*) or anti-Myc (*bottom*). The *dashed lines* indicate the mobilities of the $_{HA}ML1$ and $ML1_{Myc}$ fragments generated from wild-type ML1 (*WT*) relative to those of the mutant constructs. The migration of molecular weight markers is noted on the *left* of each gel.

abolishment of the second *N*-glycosylation consensus sequence affected the mobility of the N-terminal fragment (HA fragment) without disrupting the carboxyl-terminal half (Myc fragment) of the protein. In contrast, removal of the third or fourth *N*-glycan had no effect on amino-terminal mobility but resulted in a shift in MW of the carboxyl-terminal half of the protein. Interestingly, the resulting mobilities of the N220A and N230A carboxyl-terminal fragments were different, suggesting that the third and fourth glycans are normally processed somewhat differently. Such differential processing of *N*-glycans at distinct positions has previously been observed (22). These data are consistent with cleavage of ML1 at a site between the second and third *N*-glycans (amino acids 179–220).

The amino acid sequence of the interval between the second and third *N*-glycans of ML1 is shown in Fig. 4*A*. Because this sequence contains two basic residues that are potential cathepsin cleavage sites, we tested the effect on ML1 cleavage of mutating these residues to alanine. In neither mutant (R200A or K219A) was cleavage demonstrably affected (Fig. 4*B*). Moreover, overnight incubation of ML1-transfected cells with the cathepsin inhibitors E-64d (2 μM) (data not shown) or CA-074-Me (2 μM) (Fig. 4*C*), a more selective inhibitor of cathepsins B and L, did not reproducibly inhibit ML1 cleavage as detected either on immunoblots (Fig. 4*C*, *left*) of cell lysates or in metabolically labeled cells treated with inhibitor during the pulse and chase periods of the experiment (Fig. 4*C*, *right*). However, treatment of ML1-transfected cells with 20 μM leupeptin, which inhibits a broad spectrum of lysosomal serine, plasmin, and cysteine proteases, significantly reduced the amount of ML1 cleavage products detected in immunoblots and in metabolically labeled cells (Fig. 4*C*). Thus, it appears that cathepsins are not solely responsible for ML1 cleavage, although it is possible that multiple proteases may be able to cleave within this region.

Adaptor Protein-dependent Trafficking of ML1—Both the amino and carboxyl termini of ML1 contain several motifs that fit the consensus for AP complex binding, including tyrosine tetrapeptide Y*XX*Φ (where Φ represents a hydrophobic residue) and dileucine motifs (Fig. 4*A*). To date, three of the four AP complexes in cells (AP-1, AP-2, and AP-3) as well as the Golgi-localized, γ-ear-containing, ARF-binding (GGA) proteins have been implicated in the biosynthetic delivery of membrane proteins to late endosomes/lysosomes (reviewed in Ref. 23). In previous studies, it has been speculated that the C-terminal dileucine motif E^{574}HSLLVN functions as the lysosomal targeting signal of ML1 (5, 10). This sequence is reminiscent of the consensus motif for protein binding to the VHS domain of the GGAs (D*XX*LL, typically located 1–2 residues from the carboxyl terminus) (23). The aspartic acid residue within this binding motif cannot be substituted even with another negatively charged residue (24); however, the murine ML1 sequence fits this consensus exactly. Therefore, we tested whether the tail of human ML1 is able to interact with the VHS domains of GGAs *in vitro*. A glutathione *S*-transferase fusion of the cytoplasmic tail was unable to bind the VHS domain of GGA-1, GGA-2, or GGA-3, suggesting that GGA-mediated sorting is not involved in biosynthetic delivery of ML1 (data not shown). To test the role of this sequence in lysosomal targeting of ML1 directly, we examined the localization of a mutant version of ML1 (ΔLLVN), which lacks the carboxyl-terminal four amino acids, in transiently transfected HeLa SS6 cells. Interestingly, this mutant, like wild-type ML1, exhibited significant colocalization with the lysosomal marker lamp-2 (Fig. 5), suggesting that the carboxyl-terminal dileucine motif is not directly responsible for ML1 targeting. Consistent with a previously published report, we also observed ML1 staining in vesicular compartments that did not colocalize with lysosomal markers (10). However, in contrast with the same study, in which it was also reported that lysosomes in ML1-expressing cells were more dispersed throughout the cytoplasm than in control cells, we did not observe any reproducible effect of ML1 overexpression on the distribution of lysosomal markers. The extent and rate of proteolytic cleavage of ΔLLVN were similar to those of wild type ML1 as determined by immunoblotting and metabolic labeling experiments (data not shown).

Because GGAs do not appear to be involved in targeting of human ML1, we systematically examined the effect of ablating AP complexes on the steady state distribution of ML1 in transiently transfected cells. To dissect the role of AP-3 in ML1 targeting, we compared the distribution of ML1 expressed in control mouse fibroblasts *versus* fibroblasts derived from the *mocha* mouse that lacks functional AP-3 due to absence of the AP-3 δ subunit. The route taken by some lysosomal proteins, including lamp-2, is slightly altered in AP-3-deficient cells such that a greater fraction traffics via the plasma membrane, but the protein ultimately accumulates in lysosomal compartments (25–27). Antibody uptake experiments were performed to confirm that more lamp-2 traffics through the plasma membrane in *mocha* cells compared with control fibroblasts. After incubation of live cells with anti-lamp-2 antibody for 1 h at 37 °C, cells were fixed, permeabilized, and incubated with secondary antibodies to detect internalized antibody. As shown in Fig. 6*C*, internalized anti-lamp-2 antibody was observed in *mocha* cells but not in control fibroblasts. No staining was observed in either cell type when primary antibody was omitted from the assay.

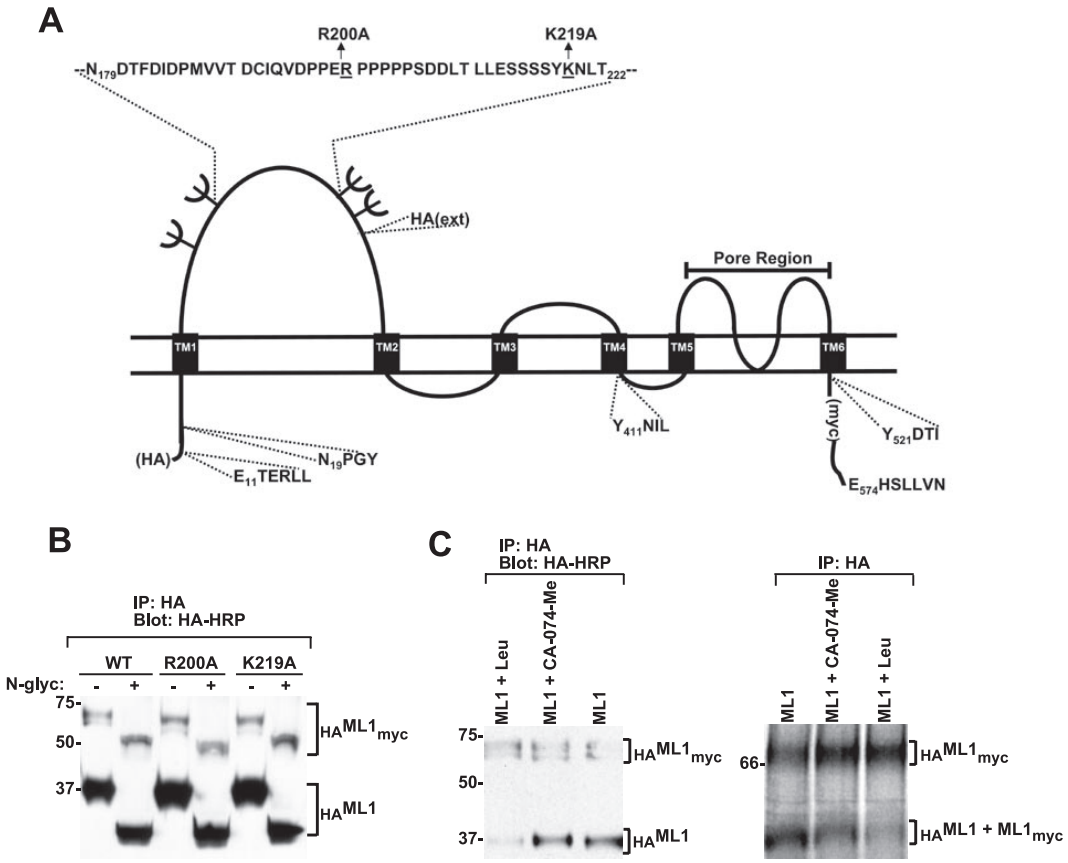

FIGURE 4. **ML1 cleavage is inhibited by leupeptin.** *A* shows a schematic representation of ML1 topology that highlights the placement of cytoplasmically disposed and external epitope tags, important potential targeting motifs, the location of *N*-glycosylation sites (*forked structures*), and the sequence of ML1 between amino acids 179 and 220. Mutations R200A and K219A that disrupt potential cathepsin cleavage sites within this region are *highlighted*. *B*, $ML1_{R200A}$ and $ML1_{K219A}$ are cleaved normally. HEK293 cells were transiently transfected with wild type or mutant ML1 constructs. Samples were immunoprecipitated (*IP*) with anti-HA antibody, mock-treated or treated with *N*-glycanase, and analyzed by immunoblotting with HRP-conjugated anti-HA. *C*, leupeptin, but not cathepsin-specific inhibitors, prevent cleavage of ML1. *Left*, leupeptin (20 μM) or the cathepsin-specific inhibitor CA-074-Me (2 μM) was added to HEK293 cells immediately after transfection and 2–3 times subsequently over the next 24 h. Cell lysates were immunoprecipitated with anti-HA antibody and immunoblotted with anti-HA antibodies. *Right*, cells were radiolabeled and then chased for 2 h either in the presence or absence of inhibitor. Cells were subsequently solubilized, immunoprecipitated with anti-HA antibodies, and electrophoresed on a 4–15% SDS-polyacrylamide gel. The migration of molecular weight markers is noted on the *left* of each gel.

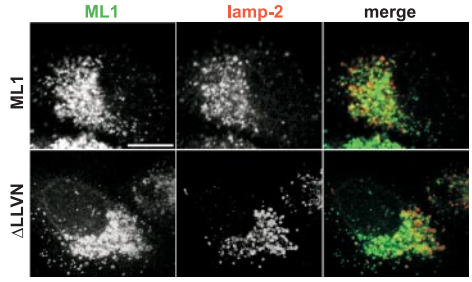

FIGURE 5. **The steady state distribution of ML1 is independent of the carboxyl-terminal LLVN sequence.** Transiently transfected HeLa SS6 cells expressing double-tagged wild-type ML1 (*top*) or $ML1_{\Delta LLVN}$ (*bottom*) were fixed and processed for double label indirect immunofluorescence to detect the N-terminal HA tag on each protein (*left*) and the lysosomal marker lamp-2 (*middle*). *Merged images* are shown in the *right-hand panels*. *Scale bar*, 10 μm.

To dissect the role of AP-3 in ML1 targeting, we used two approaches. First, we compared the steady-state distribution of ML1 by double label indirect immunofluorescence in control and *mocha* fibroblasts with that of the lysosomal marker lamp-2 (Fig. 6*A*, *top two rows*). Although ML1 in these cells was distributed in a punctate pattern reminiscent of lysosomes, there was significantly less colocalization between ML1 and lamp-2 in fibroblasts compared with HeLa cells (Fig. 5). Similar results were also obtained when the lysosomal protease cathepsin D was used as a lysosomal marker (data not shown). Second, to examine whether a greater fraction of ML1 traffics via the cell surface in *mocha* cells, we used an ML1 construct (ML1-HA(ext)) in which an HA epitope tag was inserted into the first extracellular loop of the ML1 coding sequence. Both metabolic labeling and immunoblotting experiments demonstrated that ML1-HA(ext) is biochemically processed to mature and cleaved forms, suggesting that the protein is not grossly misfolded (data not shown). Moreover, as shown in Fig. 6*A* (*bottom row*), the distribution of ML1-HA(ext) is qualitatively indistinguishable from that of the cytoplasmically tagged ML1 construct used in the *top panels* of Fig. 6*A*. However, antibody uptake experiments in 3T3 and *mocha* fibroblasts transiently expressing ML1-HA(ext) failed to reveal intracellular ML1 staining in either cell type (Fig. 6*B*). These results indicate that in the absence of functional AP-3, ML1 trafficking does not transit through the plasma membrane and suggest that ML1 trafficking is not AP-3-dependent.

To test the role of AP-1 and AP-2 in ML1 targeting, we used a siRNA knockdown approach. HeLa cells were transfected with siRNA oligonucleotides targeted against the γ-subunit of AP-1 and/or the α-subunit of AP-2 and the following day transfected with cDNA encoding epitope-tagged ML1. Immunoblotting and indirect immunofluorescence confirmed that both α- and γ-adaptin were efficiently and reproducibly knocked down by their respective siRNAs (Fig. 7). HeLa cells treated with both siRNAs and transfected with ML1 remained viable over the course of the experiment, although knockdown of both adaptins was

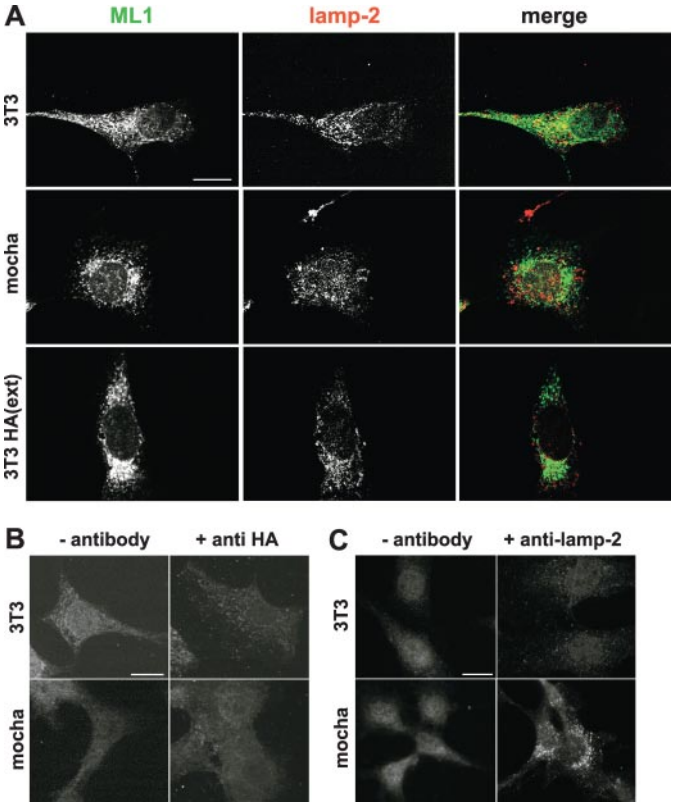

FIGURE 6. **ML1 is not mislocalized in AP-3-deficient cells.** *A*, mouse 3T3 or *mocha* fibroblasts transiently expressing cytoplasmically (*top two rows*) or 3T3 cells expressing externally tagged ML1 (ML1-HA(ext); *bottom row*) were fixed and processed for double-label indirect immunofluorescence to detect the HA tag and the lysosomal marker lamp-2. *Merged panels* are shown on the *right*. *Scale bar*, 10 μm. *B* and *C*, ML1 trafficking is not AP-3-dependent. 3T3 or *mocha* fibroblasts transiently expressing ML1-HA(ext) were incubated for 1 h at 37 °C with either anti-HA (*B*) or anti-lamp-2 (*C*) antibody. Control cells in each *panel* were incubated under identical conditions in the absence of antibody. Cells were then washed repeatedly with ice-cold PBS, fixed, and incubated with secondary antibody. Samples were viewed by confocal microscopy, and the *images* in each *panel* were acquired under identical conditions. *Scale bars*, 10 μm.

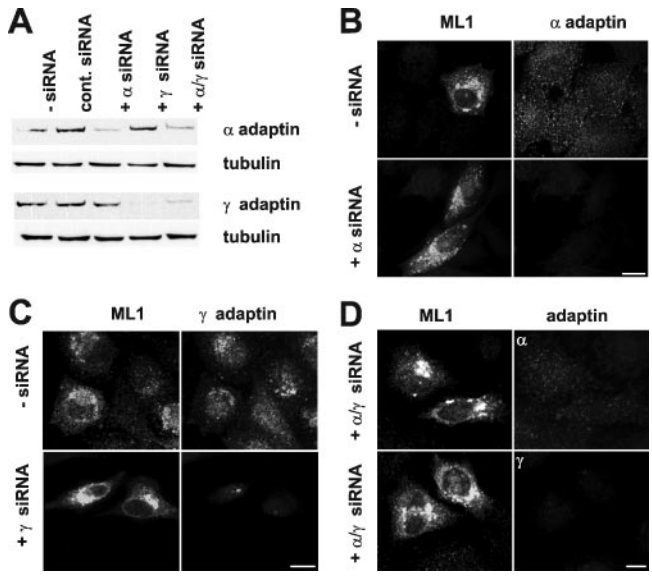

FIGURE 7. **ML1 localization is AP-1-dependent.** *A*, siRNA-mediated knockdown of α- and/or γ-adaptin. HeLa SS6 cells were mock-transfected, transfected with a control siRNA oligonucleotide, or transfected with oligonucleotides targeting α- and/or γ-adaptin. Approximately equal amounts of cell lysates (normalized by Coomassie staining) were immunoblotted to detect α- and γ-adaptin as indicated. The *bottom portion* of each gel was blotted separately to detect tubulin as an additional loading control. *B*, ML1-expressing cells that were either mock-transfected or transfected with oligonucleotides targeting α and/or γ adaptin were fixed and processed for double label indirect immunofluorescence to detect ML1 and either α-adaptin (*B*), γ-adaptin (*C*), or both (*D*) as indicated. *Scale bars*, 10 μm.

also very efficient (Fig. 7, A and D). Knockdown of α-adaptin had no effect on the distribution of ML1 (Fig. 7*B*); however, knockdown of γ-adaptin alone or in combination with α-adaptin resulted in a dramatic redistribution of ML1 (Fig. 7, *C* and *D*). In particular, whereas a significant fraction of ML1 in control cells localized to clusters of enlarged, spherical vesicles in the cytoplasm, ML1-positive vesicles were rarely observed in cells lacking γ-adaptin. To examine the distribution of ML1 in these cells further, we performed double label indirect immunofluorescence using antibodies against the HA tag on ML1 and either the *cis-/medial*-Golgi marker giantin or the soluble lysosomal hydrolase cathepsin D (Fig. 8). The half-life of cathepsin D is extremely long (>50 h) (20), and any missorted protein is secreted into the medium; thus, this protein serves as an ideal marker for lysosomes in siRNA-treated cells. In control cells, we observed significant colocalization with cathepsin D, and in particular, cathepsin D staining was frequently visualized within the lumen of ML1-positive vesicular profiles (Fig. 8*A*, *arrowheads* in *inset*). A small portion of ML1 in these cells was also observed in a ribbonlike pattern that abutted the giantin staining profile, consistent with transit of newly synthesized protein through the Golgi and *trans*-Golgi network (Fig. 8*B*). In contrast, very little colocalization of ML1 with cathepsin D could be detected in cells treated with siRNA to knock down γ-adaptin. In these cells, cathepsin D staining was largely segregated from ML1-positive compartments (Fig. 8*A*), and the majority of ML1 staining colocalized with or adjacent to giantin (Fig. 8*B*). Similar results were obtained in cells lacking both α- and γ-adaptin. Additionally, and consistent with the lack of effect of the α-adaptin knockdown on ML1 localization, we did not detect any difference in HA-antibody uptake when ML1-HA(ext) was transfected into cells treated with γ-adaptin siRNA (not shown). However, biochemical analysis by cell surface biotinylation revealed a slight increase in the amount of ML1 present at the plasma membrane in cells lacking γ-adaptin compared with control (~1% of total in control cells *versus* 2.5% of total upon γ-adaptin knockdown; data not shown). Together, these data suggest that AP-1 plays a critical role in the export of ML1 from the Golgi complex and that ML1 normally traffics to lysosomes primarily via a direct route that bypasses the plasma membrane. When γ-adaptin is knocked down, ML1 accumulates in the Golgi complex, although a small amount may traffic via the cell surface to lysosomes. Moreover, AP-3 does not appear to be able to compensate for the lack of AP-1 to target ML1 to lysosomes in cells lacking γ-adaptin.

Because depletion of γ-adaptin inhibits lysosomal delivery of ML1, we examined whether cleavage of ML1 is impaired when individual AP complexes are disrupted. Interestingly, we found no effect on ML1 cleavage relative to control in cells lacking functional AP-1, AP-2, or AP-3 (Fig. 9). Thus, cleavage of ML1 can occur in the absence of efficient delivery to late endosomes/lysosomes.

In summary, our data demonstrate that ML1 is cleaved by a leupeptin-inhibitable enzyme at a site between the second and third *N*-glycan of the first extracellular loop. Cleavage is likely to occur at a late step in the biosynthetic traffic of ML1, after maturation of the *N*-glycans. These observations are largely consistent with the recently reported findings of Kiselyov *et al.* (28). ML1 is normally delivered to lysosomes via a direct route that does not require passage through the cell surface, since knockdown of α-adaptin had no effect on the steady state distribution of ML1. Trafficking of ML1 in AP-3-deficient *mocha* cells appeared to be normal, whereas delivery of lamp-2 in these cells was disrupted. However, in these cells, we detect less overall colocalization of ML1 with

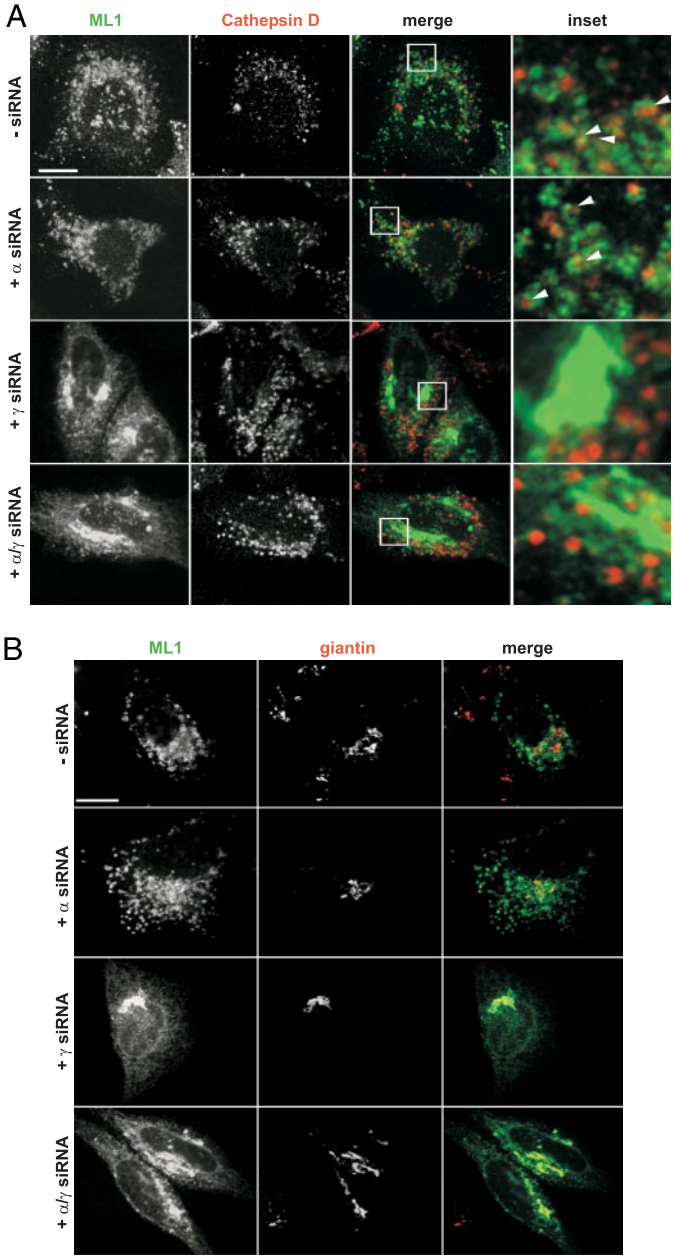

FIGURE 8. **ML1 in γ-adaptin knockdown cells is largely retained in the Golgi complex.** ML1-expressing HeLa SS6 cells that were transfected with control siRNA or with oligonucleotides targeting α- and/or γ-adaptin were fixed and processed for double label indirect immunofluorescence to detect ML1 and either the lysosomal marker cathepsin D (*A*) or the Golgi marker giantin (*B*). *Insets* in *A* show enlargements of the *boxed regions* in the *merged panels*. The *arrowheads* highlight cathepsin D staining within ML1-positive vesicles in control and α-adaptin knockdown cells. In contrast, the ML1 and cathepsin D staining profiles did not overlap significantly in cells lacking γ-adaptin or in double knockdown cells. In these cells, ML1 was observed largely concentrated in juxtanuclear regions that are coincident with giantin staining. *Scale bar*, 10 μm.

various lysosomal markers. Interestingly, cleavage of ML1 was not prevented when access to lysosomes was prevented by siRNA-mediated knockdown of AP-1. Under these conditions, the majority of ML1 accumulated in the Golgi complex, suggesting that cleavage of ML1 normally occurs prior to lysosomal delivery and possibly in the *trans*-Golgi network.

Since ML1 targeting to lysosomes involves AP-1 but does not require the carboxyl-terminal D*XX*LL-type dileucine motif, what constitutes the AP-1 recognition sequence? There are two tyrosine-containing sequences within cytoplasmically disposed regions of ML1 that fit the

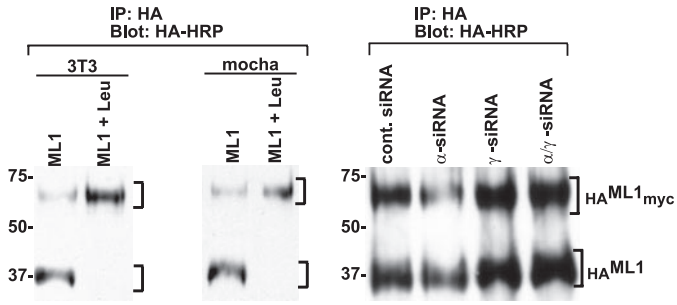

FIGURE 9. **Cleavage of ML1 is unimpaired in cells lacking functional adaptor protein complexes.** *A*, epitope-tagged ML1 was transiently expressed in 3T3 or *mocha* fibroblasts (*left*), or in HeLa cells transfected with the indicated siRNA oligonucleotides (*right*). Leupeptin (20 μM) was added to the indicated samples after transfection to inhibit cleavage of ML1. After solubilization, samples were immunoprecipitated (*IP*) using anti-HA antibody and detected by immunoblotting using HRP-conjugated anti-HA antibody. Full-length ML1 and the amino-terminal cleavage product are indicated.

Y*XX*Φ motif; however, one of these (Y^{521}DTI) is predicted to reside partly within the final transmembrane domain, and the other (Y^{411}NIL) begins two amino acids after the fourth transmembrane domain. Neither of these sequences is optimally placed for access by AP complexes (29); moreover, both are predicted to have relatively poor affinity for AP-1 (30). Another AP-1 binding candidate is an adaptor binding (D/E)*XXX*L(L/I)-type dileucine motif present at the amino terminus (E^{11}TERLL). We have detected palmitoylation of the amino terminus of ML1 *in vivo*, and this modification might also contribute to the targeting of the protein.[4] In addition, a potential adaptor-binding NP*X*Y motif (N^{19}PGY) is also present nearby; however, NP*X*Y motifs do not bind to AP-1. Consistent with our results, Vergarajauregui and Puertollano (31) reported while this manuscript was under review that the amino-terminal dileucine sequence plays a key role in lysosomal targeting of ML1 and, moreover, that lysosomal delivery of ML1 occurs largely via the direct pathway. Surprisingly, however, whereas they report palmitoylation of the carboxyl-terminal region of ML1, they did not detect amino-terminal palmitoylation. Future studies will be required to resolve this discrepancy.

What is the significance of ML1 trafficking to lysosomes via the direct pathway? Recent studies suggest that ML1 is an outwardly rectifying monovalent cation channel that may function as a proton leak channel to regulate lysosomal pH (28, 32). Based on these characteristics, significant levels of surface ML1 are predicted to result in hyperpolarization of the cells and could disrupt normal cell function. Thus, trafficking to lysosomes via the direct route may be an obligatory pathway for ML1 that serves to limit its site(s) of activity.

Acknowledgments—Epitope-tagged ML1 constructs were generated by Abigail Soyombo and Shmuel Muallem and provided by Kirill Kiselyov. We thank Gudrun Ihrke, Adam Linstedt, Balraj Doray, Stuart Kornfeld, Emily Guerriero, and Nirmala SundarRaj for cell lines and reagents and Kirill Kiselyov, Matthew Hawryluk, Peter Keyel, and Rebecca Hughey for numerous helpful discussions.

REFERENCES

1. Bach, G. (2004) *Pflugers Arch.* **451,** 313–317
2. Bargal, R., Goebel, H. H., Latta, E., and Bach, G. (2002) *Neuropediatrics* **33,** 199–202
3. Bargal, R., and Bach, G. (1997) *J. Inherit. Metab. Dis.* **20,** 625–632
4. Bassi, M. T., Manzoni, M., Monti, E., Pizzo, M. T., Ballabio, A., and Borsani, G. (2000) *Am. J. Hum. Genet.* **67,** 1110–1120
5. Sun, M., Goldin, E., Stahl, S., Falardeau, J. L., Kennedy, J. C., Acierno, J. S., Jr., Bove, C., Kaneski, C. R., Nagle, J., Bromley, M. C., Colman, M., Schiffmann, R., and Slaugen-

[4] M. T. Miedel and O. A. Weisz, unpublished observation.

haupt, S. A. (2000) *Hum. Mol. Genet.* **9,** 2471–2478
6. Bargal, R., Avidan, N., Ben Asher, E., Olender, Z., Zeigler, M., Frumkin, A., Raas-Rothschild, A., Glusman, G., Lancet, D., and Bach, G. (2000) *Nat. Genet.* **26,** 118–123
7. Clapham, D. E., Runnels, L. W., and Strubing, C. (2001) *Nat. Rev. Neurosci.* **2,** 387–396
8. Montell, C. (2005) *Sci. STKE. 2005*, RE3
9. Huang, C. L. (2004) *J. Am. Soc. Nephrol.* **15,** 1690–1699
10. Manzoni, M., Monti, E., Bresciani, R., Bozzato, A., Barlati, S., Bassi, M. T., and Borsani, G. (2004) *FEBS Lett.* **567,** 219–224
11. Di Palma, F., Belyantseva, I. A., Kim, H. J., Vogt, T. F., Kachar, B., and Noben-Trauth, K. (2002) *Proc. Natl. Acad. Sci. U. S. A.* **99,** 14994–14999
12. Raychowdhury, M. K., Gonzalez-Perrett, S., Montalbetti, N., Timpanaro, G. A., Chasan, B., Goldmann, W. H., Stahl, S., Cooney, A., Goldin, E., and Cantiello, H. F. (2004) *Hum. Mol. Genet.* **13,** 617–627
13. Cantiello, H. F., Montalbetti, N., Goldmann, W. H., Raychowdhury, M. K., Gonzalez-Perrett, S., Timpanaro, G. A., and Chasan, B. (2005) *Pflugers Arch.* **451,** 304–312
14. LaPlante, J. M., Falardeau, J., Sun, M., Kanazirska, M., Brown, E. M., Slaugenhaupt, S. A., and Vassilev, P. M. (2002) *FEBS Lett.* **532,** 183–187
15. LaPlante, J. M., Ye, C. P., Quinn, S. J., Goldin, E., Brown, E. M., Slaugenhaupt, S. A., and Vassilev, P. M. (2004) *Biochem. Biophys. Res. Commun.* **322,** 1384–1391
16. Treusch, S., Knuth, S., Slaugenhaupt, S. A., Goldin, E., Grant, B. D., and Fares, H. (2004) *Proc. Natl. Acad. Sci. U. S. A.* **101,** 4483–4488
17. Fares, H., and Greenwald, I. (2001) *Nat. Genet.* **28,** 64–68
18. Piper, R. C., and Luzio, J. P. (2004) *Trends Cell Biol.* **14,** 471–473
19. Wang, W., and Malcolm, B. A. (1999) *BioTechniques* **26,** 680–682
20. Faust, P. L., Wall, D. A., Perara, E., Lingappa, V. R., and Kornfeld, S. (1987) *J. Cell Biol.* **105,** 1937–1945
21. Traub, L. M., Kornfeld, S., and Ungewickell, E. (1995) *J. Biol. Chem.* **270,** 4933–4942
22. Machamer, C. E., Florkiewicz, R. Z., and Rose, J. K. (1985) *Mol. Cell Biol.* **5,** 3074–3083
23. Bonifacino, J. S., and Traub, L. M. (2003) *Annu. Rev. Biochem.* **72,** 395–447
24. Chen, H. J., Yuan, J., and Lobel, P. (1997) *J. Biol. Chem.* **272,** 7003–7012
25. Yang, W., Li, C., Ward, D. M., Kaplan, J., and Mansour, S. L. (2000) *J. Cell Sci.* **113,** 4077–4086
26. Janvier, K., and Bonifacino, J. S. (2005) *Mol. Biol. Cell* **16,** 4231–4242
27. Dell'Angelica, E. C., Shotelersuk, V., Aguilar, R. C., Gahl, W. A., and Bonifacino, J. S. (1999) *Mol. Cell* **3,** 11–21
28. Kiselyov, K., Chen, J., Rbaibi, Y., Oberdick, D., Tjon-Kon-Sang, S., Shcheynikov, N., Muallem, S., and Soyombo, A. (2005) *J. Biol. Chem.* **280,** 43218–43223
29. Ohno, H., Fournier, M.-C., Poy, G., and Bonifacino, J. S. (1996) *J. Biol. Chem.* **271,** 29009–29015
30. Ohno, H., Aguilar, R. C., Yeh, D., Taura, D., Saito, T., and Bonifacino, J. S. (1998) *J. Biol. Chem.* **273,** 25915–25921
31. Vergarajauregui, S., and Puertollano, R. (2006) *Traffic*, **7,** 337–353
32. Soyombo, A. A., Sang, S. T. K., Rbaibi, Y., Bashllari, E., Bisceglia, J., Muallem, S., and Kiselyov, K. (2006) *J. Biol. Chem.* **281,** 7294–7301